Electronic supplementary information

Synergistic Arsenic (V) and Lead (II) retention on synthetic jarosite. I. Simultaneous structural incorporation behaviour and mechanism

J. Aguilar-Carrillo[1*], M. Villalobos[2], T. Pi-Puig[2], I.N. Escobar-Quiroz[2], and F.M. Romero[2]

[1] Cátedra CONACyT – Department of Environmental Technology, Institute of Metallurgy, UASLP, 78210, San Luis Potosí, Mexico

[2] Department of Geochemistry, Institute of Geology, UNAM, 04510, CDMX, Mexico

[*] Author to whom correspondence should be addressed.

Phone: +52 444 8261450

email: jaguilarca@conacyt.mx

This document contains:

Text on the Synthesis procedures of solid phases

Text on the Quality control analysis and Mineral formula determination

Text on the Sample preparation for different analytical techniques

Text on the Results and Discussion of Na-, K-, and Pb-jarosites

2 Tables

2 Figures

References

Methods

2.1.1 Synthesis procedure of As-jarosites

200 mL of ultra-pure water were heated to 95 °C in a 1 L covered flask at 1 atm. Subsequently, $Fe_2(SO_4)_3 \cdot nH_2O$, KOH, and varying amounts of $Na_2HAsO_4 \cdot 7H_2O$ were added to the solution, in that order. Starting-solution compositions are summarized in Table S1; the relative As/S molar proportions in these solutions varied from 0.03 to 0.33 (0 for K- and Na-jarosites). The mixture was continuously stirred at a moderate speed (300 rpm) with a magnetic bar and held at 95 °C for 4 h. Afterwards the solution was allowed to settle at room temperature for an additional 20 h period, and the residual solution was decanted.

2.1.2 Synthesis procedure of Pb-jarosite and Pb-As-jarosites

Pb-jarosite was prepared by combining 1 L solution containing 0.054 M $Fe_2(SO_4)_3 \cdot nH_2O$ and 0.01 M H_2SO_4 with 0.03 M $Pb(NO_3)_2$. Likewise, jarosites containing both As and Pb (Pb–As-jarosites) were synthesized with the addition of varying amounts of $Na_2HAsO_4 \cdot 7H_2O$, 0.03 M HNO_3 to maintain the required pH conditions, and 0.03 M $Pb(NO_3)_2$ to yield different As/Pb initial molar ratios (Table S1). In both cases (Pb- and Pb–As-jarosite), after reaching the appropriate temperature (95 °C), 200 mL of 0.03 M $Pb(NO_3)_2$ were added dropwise to the solution at a rate of 6 mL h^{-1}, while stirring. Once all the $Pb(NO_3)_2$ had been added, the precipitates were stirred for further 5 h, after which they were allowed to settle and the residual solutions decanted.

In all cases, the precipitates obtained were rinsed five times with 200 ml ultra-pure water (18 ΩM), oven-dried for 24 h at 105-110 °C, finely ground in an agate mortar, and stored for further analysis. All chemicals employed were of analytical grade and used as received without any additional purification.

2.1.3 Synthesis procedure of amorphous ferric arsenate (AFA)

A mixture of 0.02 M As(V) ($Na_2HAsO_4 \cdot 7H_2O$) and 0.02 M Fe(III) [$Fe_2(SO_4)_3 \cdot nH_2O$] was adjusted from an initial pH of 1.3 to pH 1.8 with NaOH solution and maintained at that pH for 2 h. The solid product was separated by centrifugation, filtration, washed four times with 1 L H_2SO_4-acidified Milli-Q water (pH 2), and oven-dried at 40 °C for 96 h.

2.2 Characterization of synthetic jarosites

2.2.1 Chemical composition – quality control

Dilutions of 1:9 (w/w) were performed to ensure that the concentration of the samples was within the range of the appropriate standards for analysis. For all elemental determinations, calibration curves were run before each sample series, including matrix-matched blanks and in-between calibration checks every 10 samples to test the accuracy of the results. The calibration solutions were prepared in the same matrix as the extracting reagents from certified stock solutions. Sample blanks were analyzed for correction of background effects on instrument response. Each reported value is the average of three analyses, <5% relative difference was recorded for each sample, and <2% relative difference for quality control standards. Separate analyses of duplicate samples differed by up to ~5% for each element. The detection limits showed that concentrations in the range of a few μg L^{-1} of each of the six elements could be analyzed.

2.2.1 Chemical composition – mineral formula determination

Synthetic jarosite-like minerals bring another complication into this already rather complex group of phases. They are usually characterized by a heterogeneous deficient *B*-site (Fe^{3+} content)[1-6] as well as a deficient *A*-site occupied, besides the cationic atoms, by H_3O^+ at different proportions. For those Na-, K-, and Pb-jarosite, the occupancy of either Na^+, K^+ or Pb^{2+} in the *A*-site was fixed to the occupancy determined by ICP-OES and was constrained so that $[M^{n+} + H_3O^+] = 100\%$ or 1 atom per formula unit (a.p.f.u.), where M^{n+} refers to either Na^+, K^+, or Pb^{2+}. When the occupancy of the *A*-site was not restrained in these samples many of the formula determinations or refinements became unstable, with the occupancy of the *A*-site exceeding 100% and bond lengths becoming unreasonable.[1] For As- and Pb–As-jarosite series, we followed the same restriction of $[M^{n+} + H_3O^+] = 1$ a.p.f.u. in the *A*-site but, here, M^{n+} refers to $[Na^+ + K^+]$ and $[Na^+ + Pb^{2+}]$ respectively, according to the composition of the starting synthesis solutions (Table 1). In addition, the *T* site in Na-, K-, and Pb-jarosite is assumed to be fully occupied by sulfur atoms (S = 2 a.p.f.u.), whereas both As- and Pb–As-jarosite series were constrained on the basis of [S + As] = 2 a.p.f.u. In order to simplify the formula determination of synthesized jarosites and for the sake of comparison between phases, we consider full occupancy of *A*-site in all cases by including

the amount of hydronium (H_3O^+) needed to achieve the corresponding positive charge as a consequence of the incomplete incorporation of monovalent (Na^+, K^+) and/or divalent (Pb^{2+}) cations into the structure.[7, 8]

2.2.2 *XRD – sample preparation*

For diffraction analysis, samples were prepared following standard XRD procedures and mounted in aluminum holders. The samples were examined by XRD over a 2θ angle range of 10-70°, in step scan mode with preset time of 4s and step size of 0.02°. Mineral phase identification was made with a PDF-2 database using Shimadzu diffraction software. Crystallographic parameters of the bulk samples were calculated by Rietveld refinement of XRD spectra using TOPAS Academic v.4.1 software.[9] The specimen-dependent parameters refined were the zero error, displacement error, Chebyshev polynomial fitting for the background with six coefficients, cell parameters, crystallite size, atomic coordinates and isotropic temperature factors.

2.2.3 ATR-FTIR spectroscopy analysis – sample preparation

The diamond crystal was coated with the selected precipitate by applying a few mg of finely ground sample, evenly spread across the crystal surface, and hard-pressed with the help of a high-pressure clamp device which produced a stable deposit firmly adhered to the ATR crystal. Subsequently, a spectrum was taken as the average of 32 co-added scans at a 4 cm-1 resolution and ratioed against the bare crystal background. Spectra were co-added to improve the signal to noise ratio. The spectrometer was flushed continuously with nitrogen (N_2) to reduce the amount of CO_2 and humidity at low unvarying levels during analysis. All spectra were corrected before interpretation using the baseline correction tool. The peak position of the absorption bands was determined using Omnic v.9 software.

2.2.3 SEM observation – sample preparation

Samples were oven-dried overnight at 50 °C, embedded in low-viscosity epoxy resin (EpoThin™ 2), and finely polished with a set of gradually thinner emery papers using a commercially available low viscosity oil/water emulsion as a lubricant. Samples were also mounted on standard aluminum pin stubs and thinly coated with gold or graphite for

morphological analysis. Microprobe analysis and microprobe profiles were made with an EDAX DX4i energy dispersive spectrometry (EDS) microanalytical system on the SEM with a resolution of 3.0 nm (30 kV). The following microscopy and analytical operating conditions were used: a tilt range of -10 to +90°, an accelerating voltage of 30 kV, a working distance of 10 mm, and a specimen current range of 1pA - 1μA.

3 Results

3.1 Na-jarosite, K-jarosite and Pb-jarosite

3.1.1 X-ray powder-diffraction

Experimental procedures for the synthesis of either Na-, K-, or Pb-jarosite under acidic conditions led to the fast precipitation of a solid phase easily identified by X-ray diffraction as jarosite by comparison with the diffraction patterns International Center for Diffraction Data-Power Diffraction File (ICDD-PDF) No. 36-425, No. 22-827, and No. 39-1353 corresponding to natrojarosite, potassium jarosite and plumbojarosite respectively (Fig. S1A). The absence of additional peaks indicates that no other crystalline or poorly-crystalline phases were present at detectable levels, except for the case of Pb-jarosite where conspicuous peaks at $2\theta \approx 21°$ and 29° were attributed to anglesite ($PbSO_4$) (~5%). The presence of anglesite was also confirmed by SEM analysis (addressed later).

3.1.2 ATR-FTIR spectroscopy

All precipitates were also analyzed by ATR-FTIR and the spectra collected for Na-, K-, and Pb-jarosite matched those patterns included in the Omnic software package for natrojarosite, potassium jarosite and plumbojarosite, respectively. Briefly, all spectra have one broad peak at 3000-3600 cm^{-1} assigned to ν(O–H) modes of vibration originating from water, hydroxyl groups, and hydronium ions, appearing at lower wavenumbers for Pb-jarosite (3320 cm^{-1}) and Na-jarosite (3352 cm^{-1}) compared to K-jarosite (3378 cm^{-1}) (Fig. S1B). Other authors reported the ν(O–H) band for Pb-jarosite and Na-jarosite shifted from ours to ~3350 and ~3365 cm^{-1}, respectively, due to differences in composition.[10-12] There are also three strong peaks in the region 1000-1200 cm^{-1}: a doublet at two higher

149 wavenumbers (~1100-1200 cm^{-1}) due to the $\nu_3(SO_4^{2-})$ vibration modes of sulfate species,
150 and a singlet at ~1000 cm^{-1} assigned to the O-H deformation (δ_{OH}) coupled with $\nu_1(SO_4^{2-})$
151 vibration mode. The band near 1100 cm^{-1} is cation sensitive and occurs at a higher
152 frequency for Pb- (~1110 cm^{-1}) and Na-jarosite (~1090 cm^{-1}) than K-jarosite (~1080 cm^{-1})
153 (Fig. S1B). In all cases, additional IR bands observed near 470 and 500 cm^{-1} have been
154 assigned to lattice vibrations of FeO_6 coordination octahedra.[10]

155

156 *3.1.3 Scanning electron microscopy*

157 SEM observations of synthetic jarosites revealed differences in grain size and morphology
158 depending on the cation involved. For instance, Na- and Pb-jarosite show intergrown
159 rhombohedral (pseudocubic) crystals (Fig. S2b,c), which is characteristic of both sodium-
160 and lead-containing jarosites,[13] with diameters ranging from 1 to 5 μm in both cases. In
161 addition, as detected by XRD, anglesite orthorhombic-type crystals with 6-8 μm diameters
162 are slightly scattered in the Pb-jarosite sample (Fig. S2c). In the case of K-jarosite, grain
163 morphology ranges from subhedral to rounded and anhedral particles with 1-2 μm of
164 diameter, and sharp edges are not developed (Fig. S2a).

165

166 *3.1.4 Chemical composition*

167 As determined by ICP-OES, the atomic percentages of potassium and sodium (lead will be
168 addressed later) were lower than the theoretical values for the formula
169 $(K,Na)Fe_3(SO_4)_2(OH,H_2O)_6$, indicating a possible substitution of part of the K^+-Na^+ and
170 OH^- ions by H_3O^+ and H_2O respectively (Table 1). The resulting Na-jarosite had ~70% Na
171 occupancy whereas K-jarosite had ~85% K occupancy despite the fact that both ions were
172 at the same concentration in the starting solutions (1 M). In addition, both Na- and K-
173 jarosite have also deficiency in Fe (B-sites) with values of 2.74 and 2.79 a.p.f.u.,
174 respectively. In summary, the chemical composition of the jarosites synthesized in this
175 study are in good agreement with those reported by Basciano and Peterson[14] for Na-jarosite
176 (sample R) and by Drouet and Navrotsky[7] for K-jarosite (the one coprecipitated from KOH
177 and iron (III) sulfate in their Table 1).

In the case of Pb-jarosite, the approximately 5% anglesite present in the sample determined by XRD semi-quantitative analysis has been taken into account to recalculate the amount of Pb incorporated into the jarosite structure from the results obtained by ICP-OES. Following the same procedure for Na- and K-jarosite chemical composition determination, the average formula of synthetic Pb-jarosite used in this work was found to be $(H_3O)_{0.74}Pb_{0.13}Fe_{2.87}(SO_4)_2(OH,H_2O)_6$, which differs noticeably from the ideal stoichiometric plumbojarosite end-member $Pb_{0.5}Fe_3(SO_4)_2(OH,H_2O)_6$ despite highly similar XRD patterns.

4. Discussion

4.1 Na-jarosite, K-jarosite and Pb-jarosite

4.1.1 X-ray powder-diffraction

The simultaneous appearance of anglesite along with Pb-jarosite is frequently observed in real scenarios, i.e. mine tailings, where plumbojarosite is the principal Pb-bearing phase.[15] Basciano and Peterson[8] observed an additional weak reflection at d = 11.25 Å (equivalent to ~8° 2θ in this work) owing to the doubled c axis as a result of divalent Pb^{2+} incorporation in the jarosite structure, thus resulting in two crystallographycally different cation positions and coordination polyhedra, which are half filled with Pb cations. However, other studies did not report this reflection, even though such a distribution of Pb cations exhibits a c axis doubled in length on the unit cell, which has been observed for natural samples of plumbojarosite[16] (c = 33.675 Å). In this work, and similarly to Bartlett and Nocera[17], there is no diffraction feature at $d \approx 11$ Å (~8° 2θ) corresponding to a c-axis doubled superstructure. The first observed reflection in the powder diffraction pattern of Pb-jarosite (Fig. S1A, top) appears at ~15° 2θ, corresponding to a d_{003} typical for the interlayer distance of jarosites.[14]

4.1.2 ATR-FTIR spectroscopy

All bands observed in the ATR-FTIR spectra (Fig. S1B) are similar to those reported previously[7, 10, 11] and can be assigned to vibrations of the jarosite-type structure. The

frequency shift between Na-, Pb- and K-jarosite in the 3000-3600 cm^{-1} region can be attributed to an increase in energy of hydrogen bonds within the structure as a consequence of unit cell changes from the different ionic radii involved (r_{K+} = 1.64 Å, r_{Na+} = 1.39 Å, r_{Pb2+} = 1.21 Å),[11, 18] producing a decrease in the unit cell "c" parameter when smaller ions (Pb^{2+} and Na^{+}) are present.[7] The different band position near 1100 cm^{-1} depends on the cation involved (Na, K, or Pb) and is in good agreement with Spratt *et al*.[2], who found that these bands shifted to higher wavenumbers as the radius of the *A*-site cation decreased. Pb-jarosite shows broad and divided peaks in this region owing to the mixture of two types of SO_4, one with SO_4 adjacent to Pb^{2+} ions, and one where SO_4 is not adjacent to Pb^{2+} ions (but to vacancies or H_3O^{+}), with an extra peak at ~1070 cm^{-1} not observed in either Na- or K-jarosite, and also attributed to $\nu_3(SO_4^{2-})$.

4.1.3 Chemical composition

According to the values shown in Table 2, none of the precipitates obtained were end-member Na- or K-jarosite (Pb-jarosite will be discussed later) despite the addition of Na^{+} or K^{+} in excess in the starting solutions to reduce the H_3O^{+} ions activity. This finding, however, is a predictable result since end-member jarosite synthesis difficulties have been previously reported by some authors.[7, 19] In this study, the incomplete incorporation of Na (~70%) or K (~85%) in the *A*-site suggests that H_3O^{+} ions compete more effectively with Na^{+} than with K^{+} ions for occupancy of the *A*-sites. The similarity in solubility between natrojarosite and hydronium jarosites may also suggest an easier exchange between these ions *vs*. the exchange with K^{+}. Drouet and Navrotsky[7] reported that potassium is preferentially incorporated into the jarosite structure than sodium (and hydronium) because K-jarosite is more thermodynamically stable than the former,[20] according to end-member solubility product constants from PHREEQC,[21] which are $10^{-5.28}$ for Na-jarosite, $10^{-5.39}$ for H_3O-jarosite, and $10^{-9.21}$ for K-jarosite. For this reason, potassium-rich jarosite precipitates out of solution first, even when a very low amount of potassium is added to the solution. Our results from Visual MINTEQ and MINEQL+ geochemical modeling programs also predict the formation of jarosites with preferential incorporation of K over Na and H_3O in *A*-sites. Regarding the deficiency in Fe (*B*-sites), it has been reported that the Fe content in jarosites synthesized from dilute solutions at temperatures close to or below 100 °C (as

238 performed in this work) typically decreases from 3 a.p.f.u. to 2.20-2.57 a.p.f.u.[3-5] Therefore,
239 the existence of apparent non-stoichiometry in synthetic jarosite due to deficiencies in both
240 monovalent and trivalent cations is well established. But having less than full K^+ or Na^+ *A*-
241 site occupancy does not necessarily involve H_3O^+ structural incorporation,[22] and charge
242 neutralization to make up for a deficiency in trivalent cation can occur by the addition of
243 H^+, resulting in frequently observed *A*-site vacancies.[1, 14] In this regard, Nielsen *et al*.[6]
244 proposed that in jarosites containing Fe^{3+} site vacancies, the presence of H^+ can react with
245 the OH groups within the framework, then creating 4 Fe-OH_2 groups per Fe^{3+} site vacancy
246 and subsequent vacancy in the *A*-site would occur for only several of the *A*-sites. It is
247 common to observe as much as 10-15% vacancy in the *B*-site of jarosite in synthetic
248 studies, even up to 20%.[23] This suggests that the elusive H_3O^+ ion plays a minor role in
249 jarosite minerals than commonly assumed and, thus, it is not a key factor in formula
250 determination.[24] The fact that H_3O has been considered elusive could be explained by
251 quantum mechanics as the hydronium cation is found to occupy a lower symmetry tilted
252 orientation leading to a greater degree of disorder in the hydrogen positions. This higher
253 level of disorder in the hydrogen positions offers a reasoning as to why their location has
254 proved elusive thus far.[25] Therefore, as indicated in the Experimental Methods section and
255 for the sake of comparison between phases of this work and others reported in the literature,
256 we consider full occupancy of *A*-site in all cases by including the theoretical amount of
257 hydronium (H_3O^+) needed to achieve the corresponding positive charge in the structure.
258 In the case of Pb-jarosite (Table 2), such a level of hydronium-for-lead substitution and Fe
259 deficiency was also reported in synthetic[8, 13] and natural[4] samples. The apparent difficulty
260 to prepare a pure end-member plumbojarosite sample by synthesis at moderate temperature
261 and pressure conditions, generally involving aqueous solutions at very low pH, might find
262 crystallographic explanation due to structural changes (doubling of the *c*-axis parameter) as
263 the lead content increases. According to Basciano and Peterson[8], less than a third of the *A*-
264 site of the jarosite structure needs to be filled by Pb^{2+} in order to attain the doubling of the
265 *c*-axis parameter mentioned above to ~33.7 Å. At this lead concentration, the H_3O^+ content
266 reaches 0.34 per unit formula. Thus, the stretching effect along the *c*-axis might create a
267 miscibility gap in the solid solution between plumbojarosite and hydronium jarosite.[13]

Therefore, there is limited Pb^{2+} incorporation in the jarosite structure and charge balance is maintained by incorporating H_3O^+ since no other cations are present.

271

272 **Table S1**. Starting-solution compositions and solid molar relationships of synthesized precipitates

Sample	Molar concentrations							Aqueous molar ratios[a]		Solid molar ratios		
a) Pure jarosites	Na	K	Pb[c]	Fe	S[d]	As[e]	OH^-	As/S	As/Pb	As/(As+S)[f]	As/Pb	Fe/As
Na-jarosite	1.00	na	na	1.08	1.62	na	1.00	na	na	n.a.	n.a	
K-jarosite	na	1.00	na	1.08	1.62	na	1.00	na	na	n.a.	n.a	
Pb-jarosite	na	na	0.03	0.11	0.17	na	0.02(H^+)¥	na	na	n.a.	n.a	
b) As-jarosites[b]	Na	K	Pb	Fe	S	As	OH^-					
As-jarosite 3%	0.11	1.00	na	1.08	1.62	0.054	1.00	0.03	na	0.0223(7)	n.a	36(1)
As-jarosite 6%	0.22	1.00	na	1.08	1.62	0.108	1.00	0.06	na	0.0459(1)	n.a	19.2(4)
As-jarosite 12%	0.43	1.00	na	1.08	1.62	0.216	1.00	0.13	na	0.105(1)	n.a	9.1(1)
As-jarosite 17%	0.65	1.00	na	1.08	1.62	0.324	1.00	0.20	na	0.21(2)	n.a	5.2(1)
As-jarosite 25%	1.08	1.00	na	1.08	1.62	0.540	1.00	0.33	na	0.417(1)£	n.a	3.06(5)
c) Pb-As-jarosites[b]	Na	K	Pb	Fe	S	As	H^+					
Pb-As-jarosite 3%	0.011	na	0.03	0.108	0.162	0.0054	0.03	0.03	0.18	0.044(1)	0.77(5)	18.8(4)
Pb-As-jarosite 6%	0.022	na	0.03	0.108	0.162	0.0108	0.03	0.06	0.36	0.076(2)	1.5(2)	11.18(5)
Pb-As-jarosite 12%	0.043	na	0.03	0.108	0.162	0.0216	0.03	0.13	0.72	0.136(3)	2.3(1)	5.90(9)
Pb-As-jarosite 17%	0.065	na	0.03	0.108	0.162	0.0324	0.03	0.20	1.08	0.275(7)	4.1(3)	3.90(3)
Pb-As-jarosite 21%	0.086	na	0.03	0.108	0.162	0.0432	0.03	0.27	1.44	0.33(2)	3.6(3)	3.5(3)
Pb-As-jarosite 25%	0.108	na	0.03	0.108	0.162	0.0540	0.03	0.33	1.80	0.387(1)£	4.6(1)	3.30(3)

273 [a] Initial aqueous molar ratios.
274 [b] Numbers are increasing AsO_4 concentration in the starting solution based on $X\% = [AsO_{4(aq)}]/([AsO_{4(aq)}]+[SO_{4(aq)}])$.
275 [c] Added as $Pb(NO_3)_2$.
276 [d] Added as $Fe_2(SO_4)_3 \cdot nH_2O$.
277 [e] Added as $Na_2HAsO_4 \cdot 7H_2O$.
278 [f] Arsenate molar fraction within the jarosite structure. Computed as $[AsO_4/(AsO_4+SO_4)]$.
279 ¥ Addition of H^+ instead of OH^-.
280 £ Computed from the bulk precipitate since no jarosite was formed.
281 n.a., not applicable.
282

Table S2. Comparison of the differences in unit-cell parameters of Pb–As-jarosites arising from the incorporation of arsenic and lead

Sample[a]	As/Pb = 0.18	As/Pb = 0.36[b]		As/Pb = 0.72[b]		As/Pb = 1.08	As/Pb = 1.44
		Phase I (70%)	Phase II (30%)	Phase I (55%)	Phase II (45%)		
CELL PARAMETERS[c]							
a (Å)	7.3270(4)	7.3357(3)	7.3385(4)	7.3330(4)	7.3342(6)	7.3359(4)	7.3378(6)
c (Å)	16.8443(9)	16.8120(7)	16.8854(8)	16.7689(9)	16.876(1)	16.869(1)	16.882(1)
Cell volume (Å^3)	**783.141**(9)	**783.481**(7)	**787.52**(9)	**780.919**(9)	**786.17**(1)	**786.26**(1)	**787.19**(1)
CRITERIA OF FIT[d]							
R_{wp}	10.67	9.13		9.11		8.72	9.35
R_p	3.63	3.53		2.90		4.87	2.68
Gof	1.84	1.62		1.45		1.71	1.80

[a] Precipitates obtained from the corresponding As/Pb initial conditions.
[b] Sample was fit with two jarosite phases (see text).
[c] Estimated standard deviations in parenthesis.
[d] R_{wp} = weighted-pattern, R_p = R-pattern, Gof = Goodness of fit.

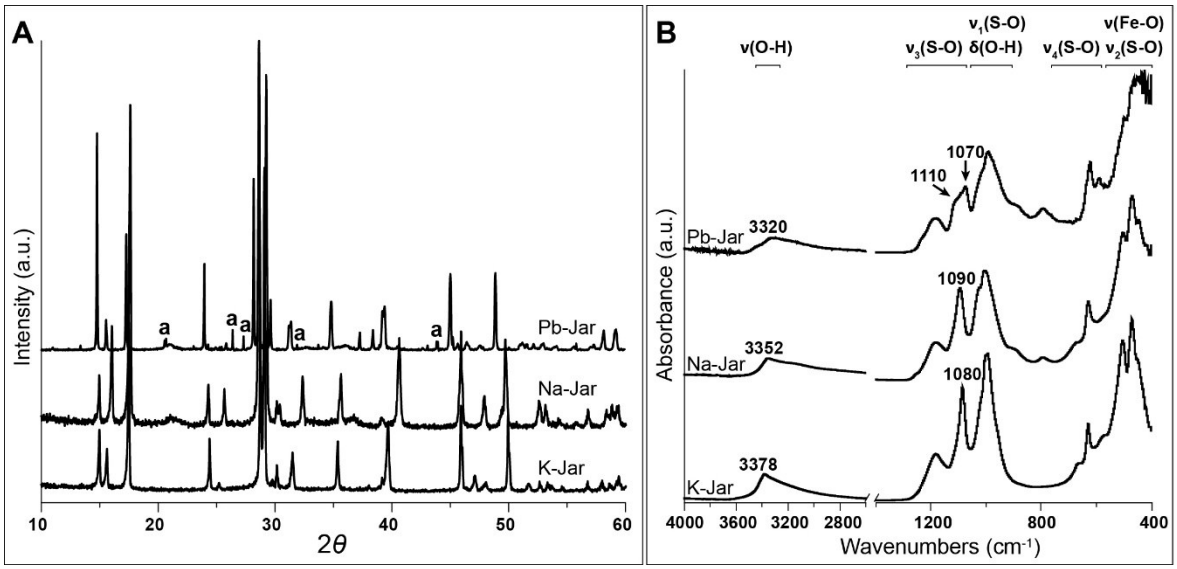

Figure S1. X-ray powder-diffraction patterns (A) and ATR-FTIR spectra (B) of synthetic K-jarosite (bottom), Na-jarosite (mid), and Pb-jarosite (top). Anglesite, occurring as a minor phase in the Pb-jarosite sample, is indicated by "a".

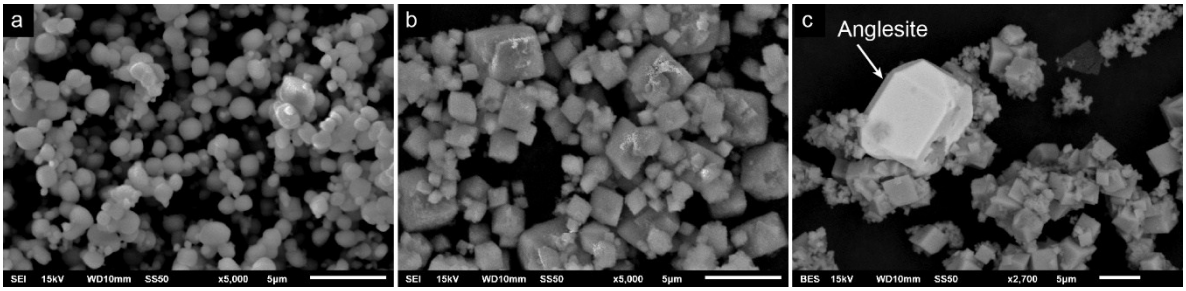

Figure S2. Scanning electron microprobe (SEM) images of synthetic (a) K-jarosite, (b) Na-jarosite, and (c) Pb-jarosite, showing morphological differences related to the main A-site cation. Anglesite, occurring as a minor phase in the Pb-jarosite sample, is indicated by an arrow.

References

1. L. C. Basciano and R. C. Peterson, Jarosite-hydronium jarosite solid-solution series with full iron site occupancy: Mineralogy and crystal chemistry, *Am Mineral,* 2007, **92**, 1464-1473
2. H. J. Spratt, L. Rintoul, M. Avdeev and W. N. Martens, The crystal structure and vibrational spectroscopy of jarosite and alunite minerals, *Am Mineral,* 2013, **98**, 1633-1643
3. C. Hartig, P. Brand and K. Bohmhammel, Fe-Al-isomorphism and structural water in crystals of jarosite-alunite-type, *Z Anorg Allg Chem,* 1984, **508**, 159-164
4. J. A. Ripmeester, C. I. Ratcliffe, J. E. Dutrizac and J. L. Jambor, Hydronium ion in the alunite-jarosite group, *Can Mineral,* 1986, **24**, 435-437
5. I. E. Grey, N. V. Y. Scarlett and H. E. A. Brand, Crystal chemistry and formation mechanism of non-stoichiometric monoclinic K-jarosites, *Mineral Mag,* 2013, **77**, 249-268
6. U. G. Nielsen, I. Heinmaa, A. Samoson, J. Majzlan and C. P. Grey, Insight into the local magnetic environments and deuteron mobility in jarosite (AFe 3(SO 4) 2(OD,OD 2) 6, A = K, Na, D 3O) and hydronium alunite ((D 3O)Al 3(SO 4) 2(OD) 6), from variable-temperature 2H MAS NMR spectroscopy, *Chem Mater,* 2011, **23**, 3176-3187
7. C. Drouet and A. Navrotsky, Synthesis, characterization, and thermochemistry of K-Na-H3O jarosites, *Geochim Cosmochim Acta,* 2003, **67**, 2063-2076
8. L. C. Basciano and R. C. Peterson, A crystallographic study of the incomplete solid-solution between plumbojarosite and jarosite, *Can Mineral,* 2010, **48**, 651-659
9. R. W. Cheary and A. Coelho, Fundamental parameters approach to x-ray line-profile fitting, *J Appl Crystallogr,* 1992, **25**, 109-121
10. K. Sasaki, O. Tanaike and H. Konno, Distinction of jarosite-group compounds by Raman spectroscopy, *Can Mineral,* 1998, **36**, 1225-1235
11. J. L. Bishop and E. Murad, The visible and infrared spectral properties of jarosite and alunite, *Am Mineral,* 2005, **90**, 1100-1107
12. R. L. Frost, R. A. Wills, M. L. Weier and W. Martens, Comparison of the Raman spectra of natural and synthetic K- and Na-jarosites at 298 and 77 K, *J Raman Spectrosc,* 2005, **36**, 435-444
13. F. L. Forray, A. M. L. Smith, C. Drouet, A. Navrotsky, K. Wright, K. A. Hudson-Edwards and W. E. Dubbin, Synthesis, characterization and thermochemistry of a Pb-jarosite, *Geochim Cosmochim Acta,* 2010, **74**, 215-224

14. L. C. Basciano and R. C. Peterson, Crystal chemistry of the natrojarosite-jarosite and natrojarosite-hydronium jarosite solid-solution series: A synthetic study with full Fe site occupancy, *Am Mineral,* 2008, **93**, 853-862
15. S. M. Hayes, S. M. Webb, J. R. Bargar, P. A. O'Day, R. M. Maier and J. Chorover, Geochemical weathering increases lead bioaccessibility in semi-arid mine tailings, *Environ Sci Technol,* 2012, **46**, 5834-5841
16. J. T. Szymanski, The crystal structure of plumbojarosite Pb[Fe3(SO4)2(OH)6]2, *Can Mineral,* 1985, **23**, 659-668
17. B. M. Bartlett and D. G. Nocera, Long-range magnetic ordering in iron jarosites prepared by redox-based hydrothermal methods, *J Am Chem Soc,* 2005, **127**, 8985-8993
18. J. E. Dutrizac and J. L. Jambor, Jarosites and their application in hydrometallurgy, *Rev Mineral Geochem,* 2000, **40**, 404-452
19. G. A. Desborough, K. S. Smith, H. A. Lowers, G. A. Swayze, J. M. Hammarstrom, S. F. Diehl, R. L. Driscoll and R. W. Leinz, editors. The use of synthetic jarosite as an analog for natural jarosite. Int Conf Acid Rock Drain, 7th; 2006; St. Louis, Missouri.
20. S. Gaboreau and P. Vieillard, Prediction of Gibbs free energies of formation of minerals of the alunite supergroup 1, *Geochim Cosmochim Acta,* 2004, **68**, 3307-3316
21. C. A. J. Appelo, D. L. Parkhurst and V. E. A. Post, Equations for calculating hydrogeochemical reactions of minerals and gases such as CO2 at high pressures and temperatures, *Geochim Cosmochim Acta,* 2014, **125**, 49-67
22. J. Majzlan, J. Plášil, R. Škoda, J. Gescher, F. Kögler, A. Rusznyak, K. Küsel, T. R. Neu, S. Mangold and J. Rothe, Arsenic-rich acid mine water with extreme arsenic concentration: Mineralogy, geochemistry, microbiology, and environmental implications, *Environ Sci Technol,* 2014, **48**, 13685-13693
23. C. Drouet, K. L. Pass, D. Baron, S. Draucker and A. Navrotsky, Thermochemistry of jarosite-alunite and natrojarosite-natroalunite solid solutions, *Geochim Cosmochim Acta,* 2004, **68**, 2197-2205
24. J. Majzlan, R. Stevens, J. Boerio-Goates, B. F. Woodfield, A. Navrotsky, P. C. Burns, M. K. Crawford and T. G. Amos, Thermodynamic properties, low-temperature heat-capacity anomalies, and single-crystal X-ray refinement of hydronium jarosite, (H3O)Fe3(SO4)2(OH)6, *Physics and Chemistry of Minerals,* 2004, **31**, 518-531
25. J. D. Gale, K. Wright and K. A. Hudson-Edwards, A first-principles determination of the orientation of H3O+ in hydronium alunite, 2010, **95**, 1109-1112